Polyhedron 72 (2014) 50–55

Contents lists available at ScienceDirect

Polyhedron

journal homepage: www.elsevier.com/locate/poly

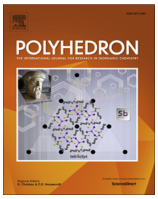

Ligand effects on the redox behavior of bimetallic tungsten(0)/ferrocene(II) complexes

Abby Moore, Kyle Shufelt, Benjamin G. Janesko, Kayla N. Green *

Department of Chemistry, Texas Christian University, 2800 S. University Dr., Fort Worth, TX 76129, United States

ARTICLE INFO

Article history:
Received 26 November 2013
Accepted 23 January 2014
Available online 31 January 2014

Keywords:
Ferrocene
Electrochemistry
Electronic effects
Infrared
Tungsten

ABSTRACT

This work presents a synthesis of bimetallic tungsten(0)/ferrocene(II) complex dppf[W(CO)$_3$PMe$_3$] and detailed comparisons of the redox behavior of dppf[W(CO)$_3$PMe$_3$], dppf[W(CO)$_4$], and dppf[W(CO)$_3$CH$_3$CN]. Reaction of PMe$_3$ with dppf[W(CO)$_3$CH$_3$CN] in dichloromethane under an inert atmosphere yields dppf[W(CO)$_3$PMe$_3$]. Slow cooling of the column purified product yields yellow blocks suitable for X-ray diffraction analysis. Structural, spectroscopic, electrochemical, and computational studies show that all three complexes have multiple redox events corresponding to tungsten and ferrocene oxidation. The complexes' distal tungsten ligands tune the first redox event over a broad range, from −37 to −200 meV versus ferrocene. Computational studies suggest that the ligand tunes the tungsten moiety's redox potential, changing the first redox event from ferrocene(II) oxidation to tungsten(0) oxidation. This bimetallic complex is thus an interesting candidate for redox-based sensing architectures.

1. Introduction

Ferrocene (Fc) derivatives have received substantial attention as electrochemical biosensors. Their redox potential can significantly shift when a molecule of interest approaches the ferrocene core [1–16]. Table 1 illustrates that the Fe$^{III/II}$ potential of ferrocene derivatives is sensitive to substituents on cyclopentadienyl (Cp). Electron donating (withdrawing) Cp substituents increase (decrease) the electron density on the iron center and yield negative (positive) shifts in redox potential. Several previous studies have treated ferrocene substituent effects [4,17–19] and bimetallic diphenylphosphinoferrocene (dppf) complexes [20–24]. Relatively few studies treat the detailed redox chemistry of bimetallic dppf complexes.

We report the first structural characterization of dppf[W(CO)PMe$_3$] (complex **3**, Chart 1) and compare its electrochemical behavior to known complexes **1** and **2**. The complexes' CO bond lengths and vibrational frequencies serve as secondary probes of ligand electron donation. The tungsten ligands' electron donor ability appears to control the redox properties, with different ligands tuning the first redox event over ~140 meV.

2. Material and methods

All reagents were purchased from commercial sources and used as received unless noted. Complex **2** was produced according to the methods reported by Hsu et al. [20,21].

2.1. Physical methods

A Varian Mercury 300 spectrophotometer was utilized to obtain the NMR spectra in deuterated solvent as specified in the sections below. UV–Vis spectra were collected on an Agilent 8453 UV–Vis spectrometer using quartz cells, and infrared spectra were obtained using a Midac Corporation FT-Infrared spectrometer.

2.2. Synthesis of 1,1′-bis(diphenylphosphine)ferrocene trimethylphosphine tungsten tricarbonyl] (*3*)

A solution of **2** (0.517 mmol, 0.446 g) and trimethylphosphine (0.8 mmol,0.8 mL) was placed in a Schlenk flask under a nitrogen blanket. Degassed CH$_2$Cl$_2$ (15 mL) solvent was added. The resulting yellow solution was stirred for 20 h. The solvent was removed under reduced pressure yielding a mixture of crude products. Products were separated via chromatography give the desired product in 89% yield (0.414 g). Chromatography used a silica column in open air and a 1:1 ratio of CH$_2$Cl$_2$: *n*-hexane as solvent. Crystals suitable for X-ray diffraction were obtained by re-dissolving the

---

* Corresponding author. Tel.: +1 817 257 6220; fax: +1 817 257 5851.
E-mail address: kayla.green@tcu.edu (K.N. Green).

http://dx.doi.org/10.1016/j.poly.2014.01.023
0277-5387/

Table 1
Measured $Fe^{III/II}$ redox potential of representative Fc derivatives.

Complex	$E_{1/2}$ (mV)
1,1′-Dibromoferrocene	337
Ferrocene (Fc)	0
Decamethylferrocene [Fe(Cp*)$_2$]	−499

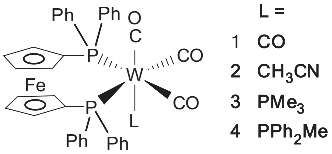

Chart 1.

product in a minimum amount of CH_2Cl_2 and cooling in a refrigerator for four days. IR spectrum (KBr pellet) ν_{CO}/cm^{-1}:1927, 1846, 1831. ^1H NMR (300 MHz, CD_3Cl, δ/ppm): 7.62–7.32 (20H, m), 4.36 (2H, m), 4.13 (2H, m), 1.02 (9H, m). ^1H NMR (300 MHz, DMSO-d_6, δ/ppm): 7.47 (20H, m), 4.472 (2H, m), 4.17 (2H, m), 0.90 (9H, m). ^{31}P NMR spectrum (CD_3Cl) δ/ppm: −43.4 (t, $J_{P-P} = 25$ Hz, $J_{W-P} = 232$ Hz) ppm, 18.3 (d, $J_{P-P} = 23$ Hz, $J_{W-P} = 214$ Hz) ppm.

2.3. Structure solution and refinement

A yellow block crystal of **3** (CCDC 967367) with approximate dimensions of 0.080 mm × 0.130 mm × 0.410 mm, was used for the X-ray crystallographic analysis. The X-ray intensity data were measured on a Bruker SMART 1000 CCD system equipped with a graphite monochromator and a Mo fine-focus tube ($\lambda = 0.71073$ Å). A total of 2400 frames were collected. The total exposure time was 13.39 h. The frames were integrated with the Bruker SAINT Software package using a SAINT algorithm. The integration of the data using a monoclinic unit cell yielded a total of 174528 reflections to a maximum θ angle of 36.41° (0.60 Å resolution), of which 18354 were independent (average redundancy 9.509, completeness = 99.7%, $R_{int} = 3.95\%$, $R_{sig} = 3.27\%$) and 14612 (79.61%) were greater than $2\sigma(F^2)$. The final cell constants of $a = 11.3247(5)$ Å, $b = 22.5717(9)$ Å, $c = 15.0822(6)$ Å, $\beta = 101.971(2)°$, volume = 3771.4(3) Å^3 are based upon the refinement of the XYZ-centroids of reflections above $20\sigma(I)$. Data were corrected for absorption effects using the multi-scan method (SADABS). The calculated minimum and maximum transmission coefficients (based on crystal size) are 0.3141 and 0.7501. The occupancy of the solvent was refined as a free variable (converged at 0.25808).

The structure was solved and refined using the Bruker SHELXTL Software Package, using the space group $P121/n1$, with $Z = 4$ for the formula unit, C40.25H37.50Cl0.50FeO3P3W. The final anisotropic full-matrix least-squares refinement on F^2 with 463 variables converged at $R_1 = 3.32\%$, for the observed data and $wR_2 = 7.04\%$ for all data. The goodness-of-fit was 1.065. The largest peak in the final difference electron density synthesis was 4.822 e Å^{-3} and the largest hole was −1.129 e Å^{-3} with an RMS deviation of 0.169 e Å^{-3}. On the basis of the final model, the calculated density was 1.619 g cm^{-3} and $F(000)$, 1826 e−.

2.4. Electrochemistry

Cyclic voltammograms were acquired at room temperature using a BASi-C3 potentiostat equipped with a 3.0 mm glassy carbon working electrode, a platinum wire auxiliary electrode, and Ag/$AgNO_3$ reference electrode filled with 0.01 M $AgNO_3$ in 0.1 M $[Bu_4N][BF_4]$ in CH_3CN. Measurements were performed under a blanket of nitrogen in 0.1 M $[Bu_4N][BF_4]$ electrolyte in CH_3CN. Measurements used a scan rate of 100 mV/s. Crystalline solid **3** required treatment with a mortar and pestle prior to dissolution. Ferrocene was used as an internal standard and reported relative to NHE (Fc/Fc^+ = +692 mV versus NHE) [25].

2.5. Computational methods

All calculations use the GAUSSIAN 09 suite of programs [26]. Calculations use nonrelativistic generalized Kohn–Sham density functional theory [27]. The noninteracting Kohn–Sham reference state wavefunction is expanded using the LANL08 basis set and relativistic effective core potential on W and Fe, and the recommended 6-311+G(d) basis on other atoms [28]. Basis sets are taken from the EMSL Basis Set Exchange [29,30]. Calculations on open-shell systems are performed spin unrestricted [31]. Stability analysis is performed on the Kohn–Sham wavefunctions [32], and the most stable SCF solution is used unless noted otherwise. DFT calculations use the local spin-density approximation LSDA [30], B3LYP [33,34], M06 [35], or ωB97X-D [36] approximate exchange–correlation functionals. All calculations use the self-consistent reaction field model for continuum acetonitrile solvent [37,38]. Calculations use M06/LANL08 geometries, vibrational frequencies, and free energy corrections. (Some test calculations use M06/LANL2DZ geometries.) Starting geometries of all complexes are taken from crystal structures and reoptimized. Geometries are optimized from the most stable electronic state. Calculated harmonic vibrational frequencies are empirically rescaled by a factor 0.9679 before comparison to experiment, following Ref. [39]. The Gibbs free energy in solution is taken as the total energy evaluated in the continuum solvent, plus ideal gas, rigid rotor, and quasiharmonic oscillator zero-point and thermal corrections evaluated at 298 K from the geometry and vibrational frequencies evaluated in continuum solvent. Put another way, the Gibbs free energy of each species is simply taken as the "Sum of electronic thermal and Free Energies" printed by GAUSSIAN 09 from a geometry optimization + vibrational frequency calculation in continuum solvent. Refs. [40–42] discuss the validity of this approach. Phenyl groups on the dppf ligand are replaced with methyl for computational convenience. Redox potentials are computed as the difference in Gibbs free energies calculated with different electron number. For example, ferrocene's $Fe^{III/II}$ redox potential is computed as the Gibbs free energy of ferrocene with charge = 1, spin multiplicity = 2; minus the Gibbs free energy of ferrocene with charge = 0, spin multiplicity = 1. Redox potentials are evaluated versus the calculated redox potential of ferrocene [43], and are compared to the experimental $E_{1/2}$ in Table 1 and the experimental Epa in Table 5. Pictures of calculated geometries use color coding C(gray), N(blue), H(white), O(red). Bond orders are drawn as a guide to the eye. Calculated spin densities are plotted with isovalue 0.0004 au.

3. Results and discussion

3.1. Structural studies

Previous studies have shown that 1,1′-bis(diphenylphosphino)ferrocene coordinates as a bidentate ligand to form octahedral tungsten complexes [11,20,21,24,44–46]. There is limited literature focusing on the redox behavior of these bimetallic systems. The current literature attributes the observed redox behavior of these systems to Fe(II), not to W(0) [24]. Here we investigate a series of dppf[W(CO)$_3$L] complexes **1**–**3** (Chart 1) [21,24]. We report the first full structural and spectroscopic characterization of **3**; and a systematic comparison of the shifts in CO bond length,

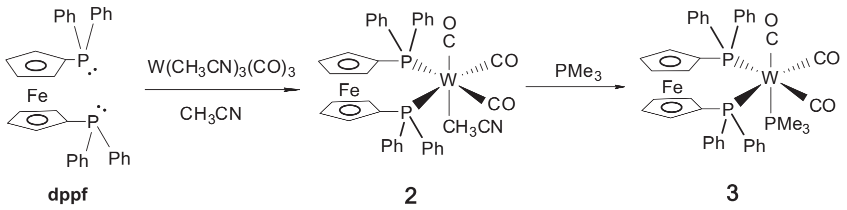

Scheme 1. Synthesis of complex **3** [21].

ν(CO), and redox potential induced by tungsten ligand L. Complex **1** was obtained commercially. Complex **2** was synthesized as shown in Scheme 1 [20,21]. Complex **3** was prepared using a modified method based on the work of Hsu and coworkers [20,21]. While **3** was prepared previously, this is the first report of its full spectroscopic and structural characterization and comparison to **1** and **2** [21].

Yellow crystals suitable for X-ray analyses were obtained from column purified **3** dissolved in dichloromethane and cooled overnight. Fig. 1 shows the single crystal X-ray diffraction structure of complex **3**. This species crystallized as a monoclinic crystal system with a space group of $P2_1/n$ derived from the four molecules each of **3** and dichloromethane solvent per unit cell. Table 2 outlines data collection and refinement details. Structural parameters of interest appear in Table 3. The Supporting Information contains full structural data. The Cp rings of the ferrocene core are arranged in a staggered fashion and provide bidentate complexation of the tungsten center. The tungsten center is roughly octahedral. The equatorial plane of tungsten atom W(1) is defined by atoms P(3), C(2), C(3) and P(2). (Fig. 1 shows atom labels.) The angles between these atoms are near 90°. The smallest angle P(1)–W(1)–C(2) is 82°, consistent with the steric effects of the bulky P(3)Ph$_2$ moiety. The W-PPh$_2$ bond lengths are largely consistent with those reported for **1** and **2**. The remaining axial ligands are largely collinear with a P(2)–W(1)–C(2) angle 170°. The three CO groups are essentially linear with W–C–O angles 174–177°. The W–CO bond lengths increase as **2** < **3** < **1**.

Table 2
Crystal data and structure refinement details for **3**.

Formula	$[C_{40}H_{37}FeO_3P_3W]_4 \cdot [CH_2Cl_2]$
Molecular weight	919.54
Unit cell	monoclinic
Space group	$P121/n1$
a (Å)	11.3247(5)
b (Å)	22.5717(9)
c (Å)	15.0822(6)
α (°)	90
β (°)	101.971(2)
γ (°)	90
Volume (Å^3)	3771.4(3)
Z	4
ρ_{calc}(mg mm^{-3})	1.619
μ (mm^{-1})	3.632
$F(000)$	1826.0
Crystal size (mm)	0.415 × 0.125 × 0.084
2θ range for data collection (°)	5.036–72.824
Index ranges	$-18 \leqslant h \leqslant 18$, $-37 \leqslant k \leqslant 37$, $-25 \leqslant l \leqslant 25$
Reflections collected	174528
Independent reflections	18354[R_{int} = 0.0393]
Data/restraints/parameters	18354/523/464
Goodness-of-fit on F^2	1.065
Final R indexes [$I > 2\sigma(I)$]	R_1 = 0.0332, wR_2 = 0.0637
Final R indexes [all data]	R_1 = 0.0531, wR_2 = 0.0704
Largest difference in peak/hole (e Å^{-3})	4.84/−1.17

An important result in Table 3 is that the tungsten ligand controls the C–O bond lengths. The average C–O bond lengths increase with increasing ligand donor character: 1.149 Å in **1**, 1.154 Å in **2**, 1.1652 Å in **3**. This indicates that the more electron donating ligands CH$_3$CN and PMe$_3$ increase tungsten-CO π backbonding. While the crystal structures are not sufficiently high resolution to unambiguously quantify these effects, the trend is consistent with shifts in ν_{CO} and redox potential discussed below. The average CO bond lengths increase as **1** < **2** < **3**, indicating that we show

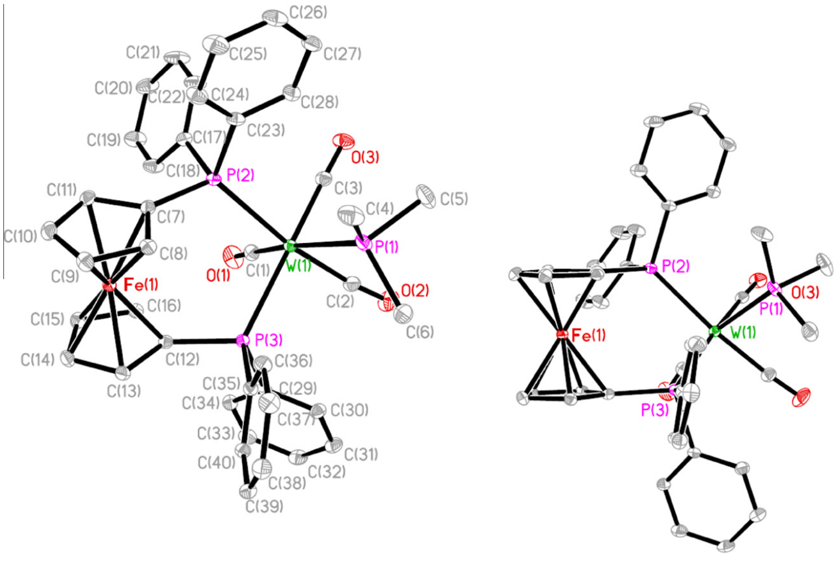

Fig. 1. Thermal ellipsoid (50% probability) plots of **3** from two viewpoints with labeling scheme.

Table 3
Comparison of bond lengths (Å) and angles (°) of interest for **1**–**3** [11,20].

			1	**2**	**3**
P2	W1	P1	–	–	98.925(6)
P2	W1	P3	95.25(7)	97.40(5)	98.429(6)
	C1	O1	1.156(9)	1.141(8)	1.1660(8)
	C2	O2	1.145(2)	1.144(8)	1.1611(9)
	C3	O3	1.153(9)	1.174(9)	1.1684(8)
	C4	O4	1.140(9)	–	–
Average	C	O	1.149	1.153	1.1652
	W1	P3	2.533(2)	2.539(2)	2.55531(17)
	W1	P2	2.563(3)	2.539(2)	2.53321(19)
	C1	W1	2.020(7)	1.906(7)	1.9703(6)
	C2	W1	1.982(9)	1.948(7)	1.9699(7)
	C3	W1	1.964(7)	1.945(8)	1.9654(7)
	C4	W1	2.029(7)	–	–
	P1	W1	–	–	2.55086(18)

below that ligand electron donation also correlates with positive shifts of the redox potential and ν_{CO} stretch frequencies.

3.2. Spectroscopic studies

The increased tungsten-CO π backbonding discussed above should decrease the C-O vibrational stretch frequencies ν_{CO} [47,48]. Table 4 reports ν_{CO} measured for complexes **1**–**3**. Complex **4** is included for comparison. Complex **1** shows three stretches assigned as $A_1{}^1$, $A_1{}^2 + B_1$, and B_2 based on the C_{2v} symmetry surrounding the tungsten center. We presume the $A_1{}^2$ and B_1 bands overlap, as seen in related Mo complexes [49,50]. Complexes **2**–**4** have a lower symmetry about the tungsten center resulting in three ν_{CO} bands. Consistent with the previous discussion, increasing tungsten ligand electron donor character (**1** < **2** < **3**) lowers ν_{CO}. The ν_{CO} of **4** are above **2** and **3**, indicating that the CH_3CN and PMe_3 ligands are more electron donating than the bulky PPh_2Me.

Table 4
ν_{CO} (cm^{-1}) and peak intensities measured for complexes **1**–**4**.

Complex	Solvent	ν_{CO}
dppfW(CO)$_4$ (**1**) (ref [24])	$CDCl_3$	2016m, 1915s, 1891vs
dppfW(CO)$_3$CH$_3$CN (**2**)	1,2-$C_2H_4Cl_2$	1930vs, 1836s, 1812s
dppfW(CO)$_3$P(Me)$_3$ (**3**)	1,2-$C_2H_4Cl_2$	1927,1846,1831
dppfW(CO)$_3$PPh$_2$Me (**4**) (ref 21)	1,2-$C_2H_4Cl_2$	1960w, 1852s, 1842(sh)

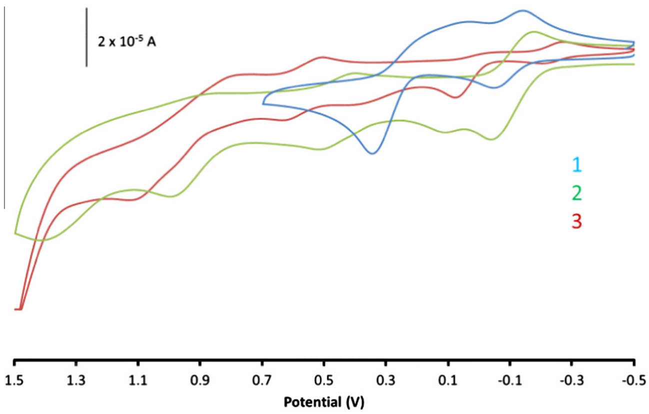

Fig. 2. Cyclic voltammograms of **1**–**3** in CH_3CN with 0.1 M $[Bu_4N][BF_4]$ at a scan rate of 100 mV/s and referenced to Fc (Fc = 0.00 mV).

Table 5
Redox peaks from Fig. 2, E_{pc} and E_{pa} represent cathodic and anodic peak potentials, other details are in Section 2.

	E_{pa} (mV)					E_{pc} (mV)	
1	−37	388				−167	
2	−40	111	517	996	1414	−176	398
3	−200	83	353	630	1123	−276	501

3.3. Electrochemical studies

Fig. 2 shows the measured cyclic voltammograms of complexes **1**–**3**. Table 5 quantifies the redox peaks from Fig. 2. The complexes show one quasi-reversible event located between 0 and −300 mV, and up to four other oxidations at more positive potentials. These presumably combine tungsten and ferrocene oxidation, ultimately yielding Fe(III)/W(IV). The most negative event had previously been attributed to oxidation of Fe(II), rather than oxidation of W(0) [24]. However, Table 5 shows that the position of this redox event sensitively depends on the tungsten ligand, with the first few peaks' E_{pa} and $E_{1/2}$ (Table SI3) decreasing with increasing ligand electron donor character as **1** > **2** > **3**. Moreover, complexes **2** and **3** show a second redox event within <120 mV of ferrocene. This suggests that the tungsten(0) species may play an important role in the complexes' electrochemistry.

3.4. Computational studies

Fig. 3 compares experimental and calculated values for the first two redox potentials of complexes **1**–**3**. For example, "3, second" refers to the second E_{pa} (83 mV versus Fc) tabulated for complex **3** in Table 5. Calculations on the molecules of Table 1 are included for comparison. The calculations reproduce the experimental trends. The R^2 and root-mean-square error between experimental and calculated redox potentials versus Fc are 0.76 and 0.25 eV. These discrepancies arise from the continuum solvent model employed, the finite basis set, the approximate exchange–correlation functional, and the experimental error bars. The RMS error is consistent with a recent computational study of monometallic complexes' one-electron redox potentials versus Fc, while the R^2 is somewhat lower [41]. The lower correlation coefficient is in part because the calculated redox potentials of W/Fe complexes **1**–**3** lie somewhat above the trend for ferrocenes, possibly due to different scaling factors for tungsten. Supporting Information Tables

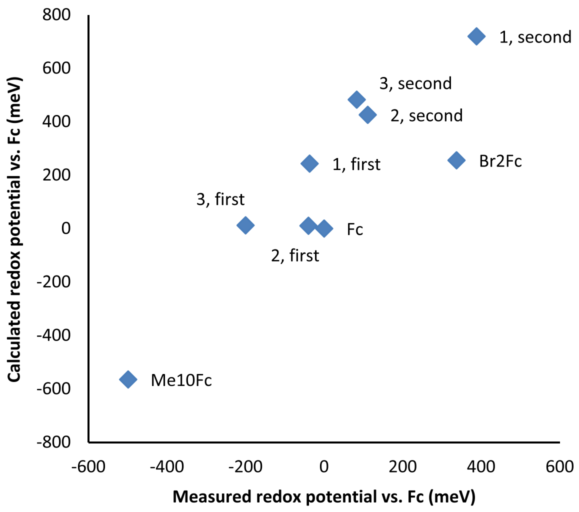

Fig. 3. Calculated vs. measured redox potentials.

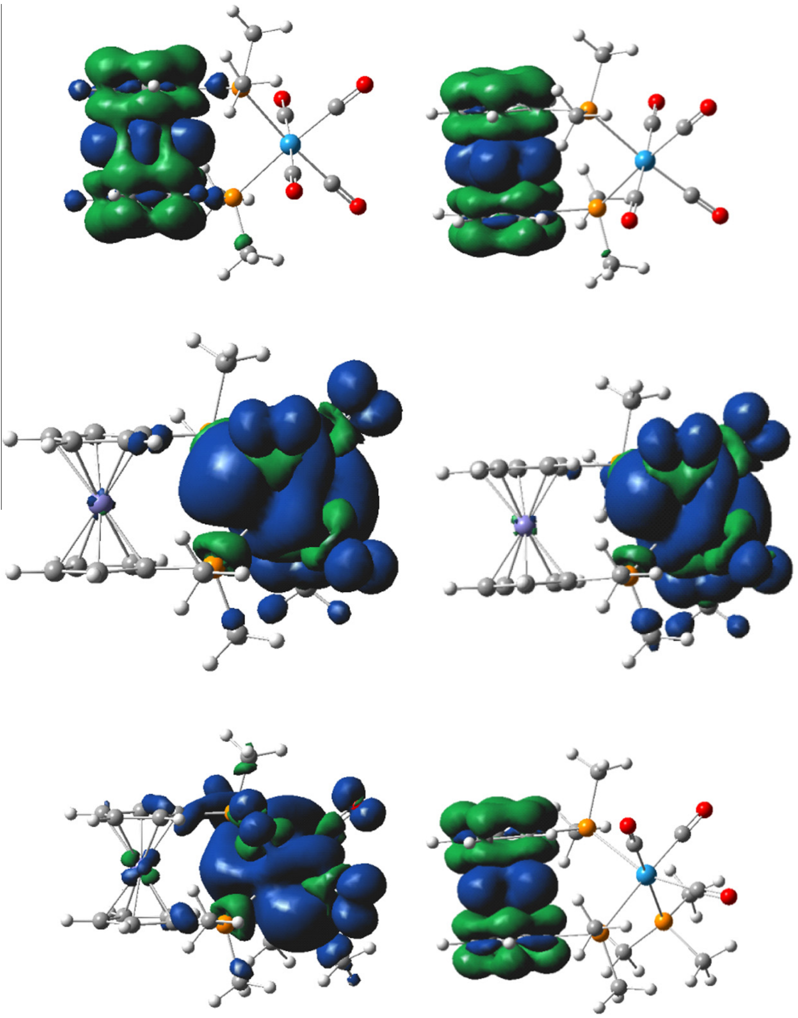

Fig. 4. Calculated M06/LANL08 (left) and ωB97XD/LANL08//M06/LANL2DZ (right) electron spin densities. One-electron-oxidized 1 (top), 2 (middle), 3 (bottom).

SI4–SI5 show that M06/LANL08 calculations also reproduce bond lengths, bond angles, and ν_{CO} of complexes **1**–**3** to within approximately 0.05 Å, 4°, and 20 cm^{-1}. These relatively small errors suggest that this level of theory is appropriate for initial computational studies. Calculations moving ligand L to the equatorial position (Fig. SI1) find that, for neutral Fe(II)/W(0), this isomer is destabilized by 12.1 kcal/mol for **2** and by 8.0 kcal/mol for **3**.

Fig. 4 illustrates a possible explanation for the tungsten ligand dependence of the first redox event. The left column of Fig. 4 shows the calculated M06/LANL08 electron spin density for one-electron-oxidized molecules **1**–**3**. The unpaired electron is localized to Fe in **1** and to W in **2** and **3**. The latter species are thus predicted to be Fe(II)/W(I) complexes, rather than Fe(III)/W(0). This suggests that the tungsten ligand dependence is not a long-range effect on ferrocene oxidation, but a tuning of the tungsten(0) moiety. The spin localization is quite sensitive to the computational method employed. The right column column illustrates this for DFT calculations with the long-range-corrected ωB97XD functional. (Supporting Information Table SI6 shows that ωB97XD/LANL08//M06L/LANL08 calculations also recover the experimental trends of Fig. 3, though the absolute values differ.) ωB97XD predicts that **2** is Fe(II)/W(I) while **1** and **3** are Fe(III)/W(0). Supporting Information Fig. SI2 shows that the LSDA predicts that all spin densities are delocalized over both metal centers, consistent with its well-known tendency to overdelocalize electrons. The oxidized, open-shell bimetallic complexes treated here are likely multideterminant, and DFT calculations may not even be qualitatively correct. However, these results provide additional evidence that the first redox event may not always be ferrocene oxidation.

4. Conclusions

The structures, infrared spectra, and electrochemistry of dppf[W(CO)$_3$R] (R = CO, CH_3CN, PMe_3) complexes were investigated to explore these complexes' complicated redox spectra. Results were supported by electronic structure calculations. The results indicate that these bimetallic Fe(II)/W(0) complexes have complex and highly tunable redox chemistry, with tungsten oxidation potentially playing a significant role. This makes them interesting candidates for future studies, particularly as redox-active sensors.

Acknowledgments

K.G. was supported by the R.A. Welch Foundation grant P-1760 and TCU Research and Creative Activities Fund. K.G. and B.G.J. were additionally supported by TCU start-up funds, and K.S. was supported by a TCU SERC grant. The authors thank Tracy Hanna for useful discussions.

Appendix A. Supplementary data

CCDC 967367 contains the supplementary crystallographic data for compound **3**. These data can be obtained free of charge via http://www.ccdc.cam.ac.uk/conts/retrieving.html, or from the Cambridge Crystallographic Data Centre, 12 Union Road, Cambridge CB2 1EZ, UK; fax: +44 1223 336 033; or email: deposit@ccdc.cam.ac.uk. Supplementary data associated with this article can be found, in the online version, at http://dx.doi.org/10.1016/j.poly.2014.01.023.

References

[1] M. Alfonso, A. Tarraga, P. Molina, Dalton Trans. 39 (2010) 8637.
[2] C. Bucher, C.H. Devillers, J.-C. Moutet, G. Royal, E. Saint-Aman, New J. Chem. 28 (2004) 1584.
[3] K. Heinze, M. Schlenker, Eur. J. Inorg. Chem. 2004 (2004) 2974.
[4] N. Husken, G. Gasser, S.D. Koster, N. Metzler-Nolte, Bioconjugate Chem. 20 (2009) 1578.
[5] S.J. Kwon, E. Kim, H. Yang, J. Kwak, Analyst 131 (2006) 402.
[6] H.T. Niu, Z. Yin, D. Su, D. Niu, J. He, J.P. Cheng, Dalton Trans. (2008) 3694.
[7] S. Prabhulkar, S. Alwarappan, G.D. Liu, C.Z. Li, Biosens. Bioelectron. 24 (2009) 3524.
[8] G.-Y. Qing, T.-L. Sun, F. Wang, Y.-B. He, X. Yang, Eur. J. Org. Chem. (2009) 841.
[9] T. Romero, A. Caballero, A. Espinosa, A. Tarraga, P. Molina, Dalton Trans. (2009) 2121.
[10] G. Sathyaraj, D. Muthamilselvan, M. Kiruthika, T. Weyhermüller, B.U. Nair, J. Organomet. Chem. 716 (2012) 150.
[11] L.C. Song, J.T. Liu, Q.M. Hu, G.F. Wang, P. Zanello, M. Fontani, Organometallics 19 (2000) 5342.
[12] S. Tanaka, K. Yoshida, H. Kuramitz, K. Sugawara, H. Nakamura, Anal. Sci. 15 (1999) 863.
[13] A. Thakur, S. Sardar, S. Ghosh, Inorg. Chem. 50 (2011) 7066.
[14] F. Zapata, A. Caballero, A. Espinosa, A. Tarraga, P. Molina, Inorg. Chem. 48 (2009) 11566.
[15] F. Zapata, A. Caballero, P. Molina, A. Tarraga, Sensors (Basel) 10 (2010) 11311.
[16] S. Zhang, F. Zheng, Z. Wu, G. Shen, R. Yu, Biosens. Bioelectron. 24 (2008) 129.
[17] D.W. Hall, C.D. Russel, J. Am. Chem. Soc. 89 (1967) 2316.
[18] W.E. Britton, R. Kashyap, M. Elhashash, M. Elkady, M. Herberhold, Organometallics 5 (1986) 1029.
[19] K. Mahmoud, Y.-T. Long, G. Schatte, H.-B. Kraatz, J. Organomet. Chem. 689 (2004) 2250.
[20] S.C.N. Hsu, W.Y. Yeh, M.Y. Chiang, J. Organomet. Chem. 492 (1995) 121.
[21] S.C.N. Hsu, W.Y. Yeh, J. Chem. Soc. – Dalton Trans. (1998) 125.
[22] T.S.A. Hor, L.T. Phang, J. Organomet. Chem. 373 (1989) 319.
[23] M.F. Farona, J.G. Grassell, B.L. Ross, Spectrochim. Acta, Part A – Mol. Spectrosc. A 23 (1967) (1875).
[24] A.C. Ohs, A.L. Rheingold, M.J. Shaw, C. Nataro, Organometallics 23 (2004) 4655.
[25] N.G. Connelly, W.E. Geiger, Chem. Rev. 96 (1996) 877.
[26] M.J. Frisch, G.W. Trucks, H.B. Schlegel, G.E. Scuseria, M.A. Robb, J.R. Cheeseman, G. Scalmani, V. Barone, B. Mennucci, G.A. Petersson, H.C. Nakatsuji, M., X. Li, H.P. Hratchian, A.F. Izmaylov, J. Bloino, G. Zheng, J.L. Sonnenberg, M. Hada, M. Ehara, K. Toyota, R. Fukuda, J. Hasegawa, M. Ishida, T. Nakajima, Y. Honda, O. Kitao, H. Nakai, T. Vreven, J.A. Montgomery, J.E. Peralta, F. Ogliaro, M. Bearpark, J.J. Heyd, E. Brothers, K.N. Kudin, V.N. Staroverov, T. Keith, R. Kobayashi, J. Normand, K. Raghavachari, A. Rendell, J.C. Burant, S.S. Iyengar, J. Tomasi, M. Cossi, N. Rega, J.M. Millam, M. Klene, J.E. Knox, J.B. Cross, V. Bakken, C. Adamo, J. Jaramillo, R. Gomperts, R.E. Stratmann, O. Yazyev, A.J. Austin, R. Cammi, C. Pomelli, J.W. Ochterski, R.L. Martin, K. Morokuma, V.G. Zakrzewski, G.A. Voth, P. Salvador, J.J. Dannenberg, S. Dapprich, A.D. Daniels, O. Farkas, J.B. Foresman, J.V. Ortiz, J. Cioslowski, D.J. Fox, Gaussian Inc, 2010.
[27] A. Seidl, A. Gorling, P. Vogl, J.A. Majewski, M. Levy, Phys. Rev. B 53 (1996) 3764.
[28] L.E. Roy, P.J. Hay, R.L. Martin, J. Chem. Theory Comput. 4 (2008) 1029.
[29] D. Feller, J. Comput. Chem. 17 (1996) 1571.
[30] K.L. Schuchardt, B.T. Didier, T. Elsethagen, L.S. Sun, V. Gurumoorthi, J. Chase, J. Li, T.L. Windus, J. Chem. Inf. Model. 47 (2007) 1045.
[31] J.P. Perdew, A. Ruzsinszky, L.A. Constantin, J.W. Sun, G.I. Csonka, J. Chem. Theory Comput. 5 (2009) 902.
[32] R. Seeger, J.A. Pople, J. Chem. Phys. 66 (1977) 3045.
[33] A.D. Becke, J. Chem. Phys. 98 (1993) 5648.
[34] P.J. Stephens, F.J. Devlin, C.F. Chabalowski, M.J. Frisch, J. Phys. Chem. 98 (1994) 11623.
[35] Y. Zhao, D.G. Truhlar, Theoret. Chem. Acc. 120 (2008) 215.
[36] J.D. Chai, M. Head-Gordon, J. Chem. Phys. 128 (2008) 084106.
[37] S. Miertus, E. Scrocco, J. Tomasi, Chem. Phys. 55 (1981) 117.
[38] E. Cances, B. Mennucci, J. Tomasi, J. Chem. Phys. 107 (1997) 3032.
[39] M.P. Andersson, P. Uvdal, J. Phys. Chem. A 109 (2005) 2937.
[40] Y. Kim, J.R. Mohrig, D.G. Truhlar, J. Am. Chem. Soc. 132 (1082) (2010) 11071.
[41] R.F. Ribeiro, A.V. Marenich, C.J. Cramer, D.G. Truhlar, J. Phys. Chem. B 115 (2011) 14556.
[42] J.M. Ho, A. Klamt, M.L. Coote, J. Phys. Chem. A 114 (2010) 13442.
[43] L.E. Roy, E. Jakubikova, M.G. Guthrie, E.R. Batista, J. Phys. Chem. A 113 (2009) 6745.
[44] J.L. Hess, H.L. Conder, K.N. Green, M.Y. Darensbourg, Inorg. Chem. 47 (2008) 2056.
[45] M. Sekino, M. Sato, A. Nagasawa, K. Kikuchi, Organometallics 13 (1994) 1451.
[46] S. Ninoreille, R. Broussier, R. Amardeil, M.M. Kubicki, B. Gautheron, Bull. Soc. Chim. Fr. 132 (1995) 128.
[47] M.L. Golden, C.M. Whaley, M.V. Rampersad, J.H. Reibenspies, R.D. Hancock, M.Y. Darensbourg, Inorg. Chem. 44 (2005) 875.
[48] M.V. Rampersad, S.P. Jeffery, M.L. Golden, J. Lee, J.H. Reibenspies, D.J. Darensbourg, M.Y. Darensbourg, J. Am. Chem. Soc. 127 (2005) 17323.
[49] D.J. Darensbourg, M.Y. Darensbourg, J. Chem. Educ. 51 (1974) 787.
[50] D.J. Darensbourg, M.Y. Darensbourg, J. Chem. Educ. 47 (1970) 33.